

Fig S1

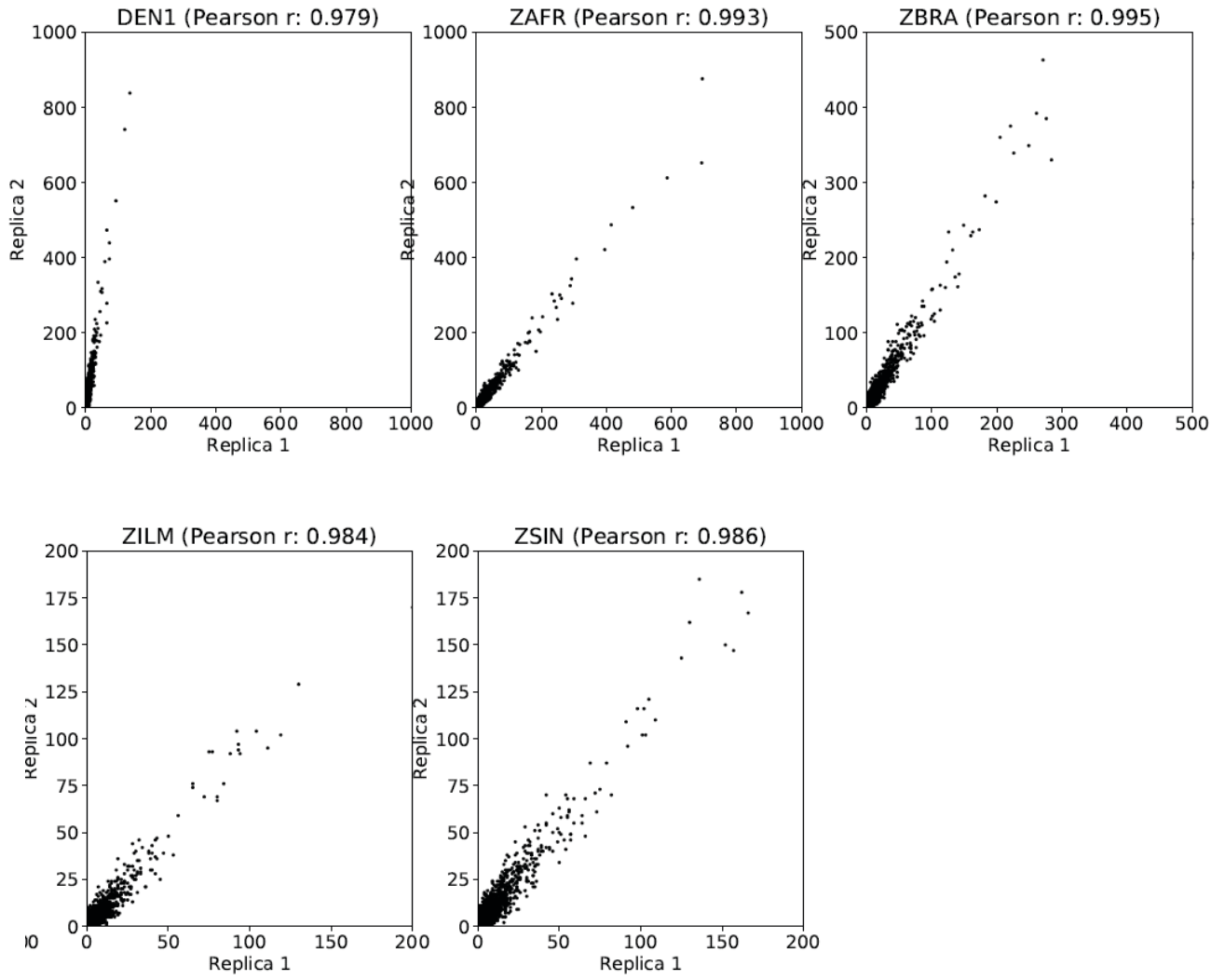


Figure S1. Quality metrics of SPLASH virus-host intermolecular interactions. Analysis of biological replicates reveals consistent interaction counts between replicates for DENV and ZIKV. Hence, replicates were subsequently pooled for further analysis.

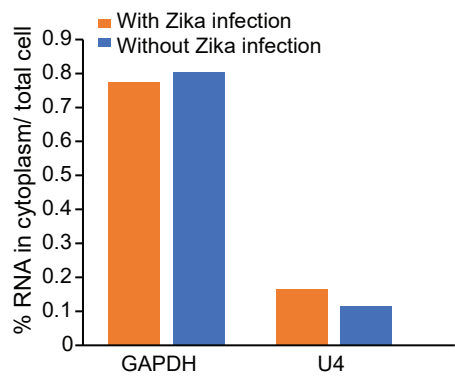
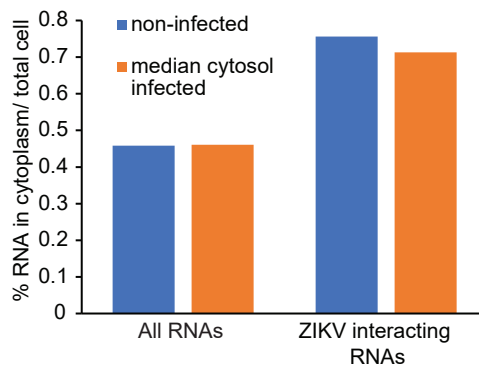
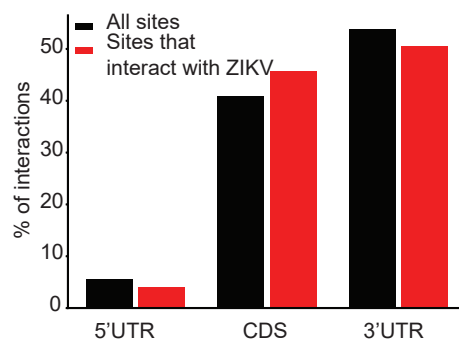
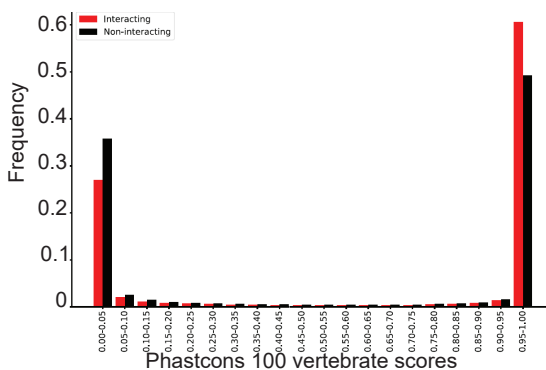
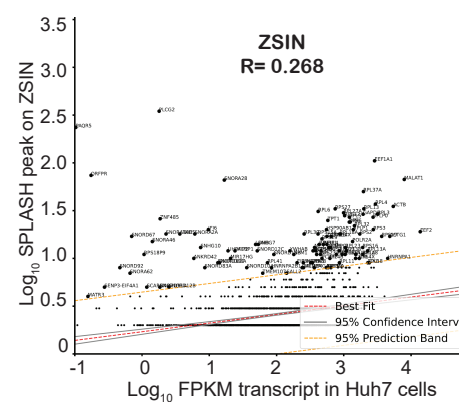
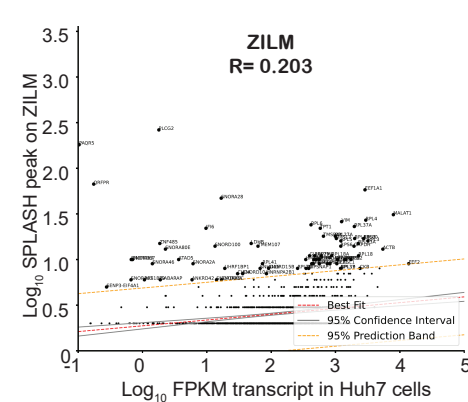
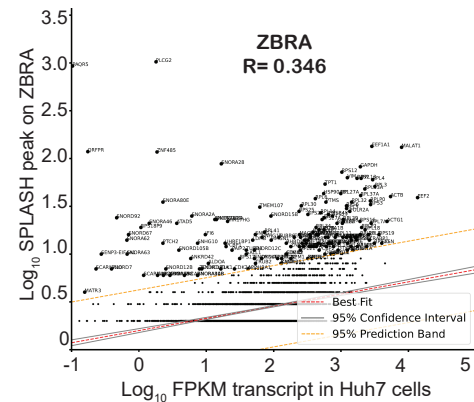
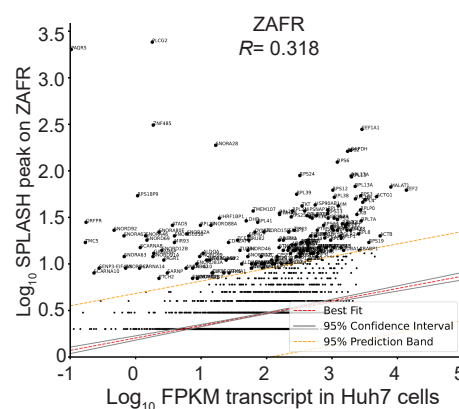
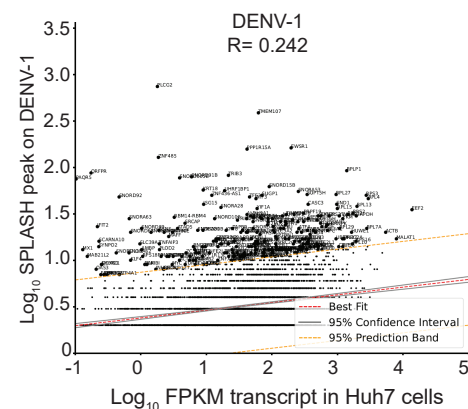
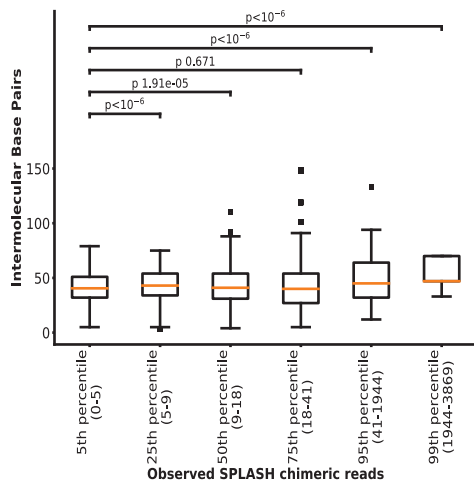
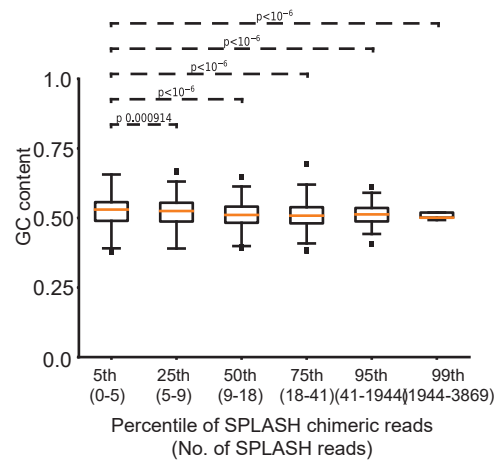
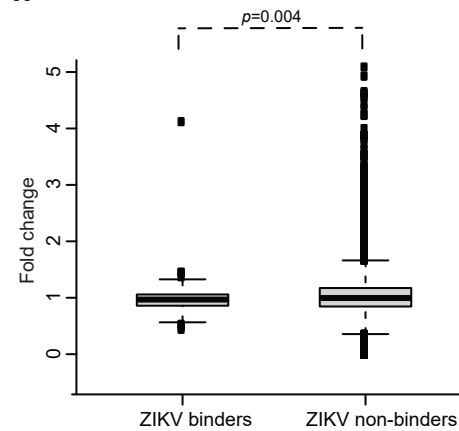
Fig S2**a****b****c****d****e****f****g****h**

Figure S2. Features of ZIKV- host RNA interactions. **a**, Bar plots showing the percentage of GAPDH and U4 RNAs present in the cytosol versus in whole cell lysate, with (orange) and without (blue) Zika infection. **b**, Bar plots showing the percentage of RNA in cytosol versus whole cell lysate for all detected RNAs in the cell and for ZIKV interacting RNAs, with (orange) and without (blue) ZIKV infection. **c**, Analysis of interacting locations reveal no preference for 5' UTR, coding sequence, or 3' UTR regions. **d**, Histogram showing the distribution of Phastcons scores for 100 vertebrates for bases that are interacting versus non-interacting with ZIKV. **e**, Correlation of RNA transcript abundance (RPKM) with the number of virus interaction counts (SPLASH counts) for detected RNAs in the cell. We did not observe a strong correlation between transcript abundance and SPLASH interaction counts indicating that transcript abundance is not the main factor in driving virus-host RNA interactions. **f**, Boxplot showing the distribution of the number of paired bases between ZIKV and its interacting host RNAs at different quantiles of SPLASH interaction counts. The number of intermolecular base pairs of the interacting regions shows that highly interacting transcripts identified by SPLASH interact with each other with longer stretches of paired bases, as expected by energetics. **g**, GC content of the interacting regions is higher for strongly interacting transcripts. In agreement with observed energetics, increased GC content in the interaction region correlates with higher observed read counts. **h**, Boxplots showing the distribution of gene expression changes in host RNAs that bind (left) and does not bind (right) to the ZIKV genome, after the cells are infected with ZIKV for 24 hrs.

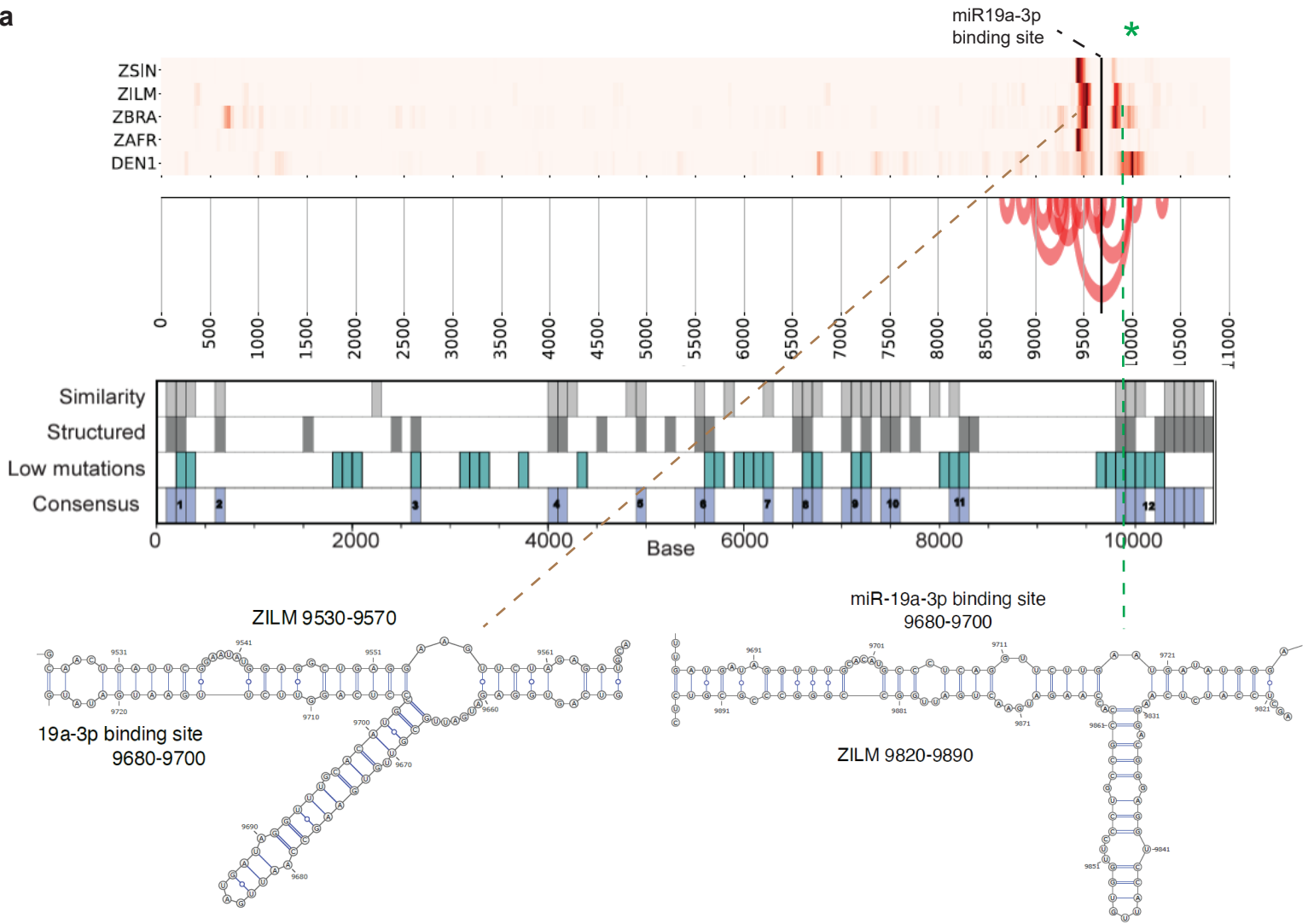
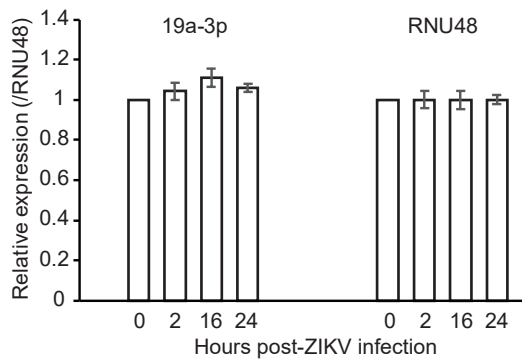
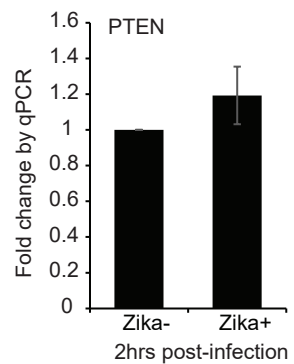
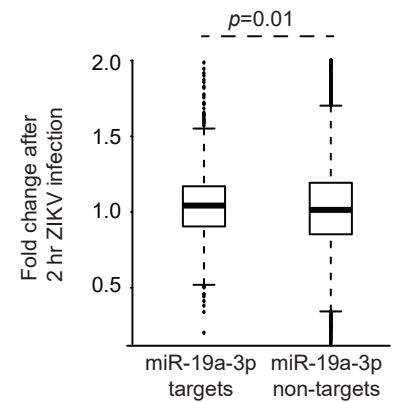
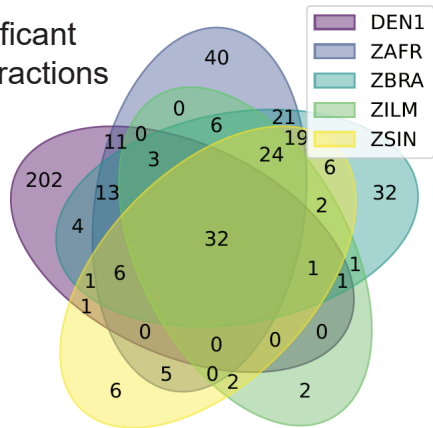
Fig S3**a****b****c****d**

Figure S3. ZIKV:miRNA interaction statistics. **a**, Top: Heatmap showing the bases along the ZIKV-ILM genome that interacts with the miR-19a-3p binding site. The black line represents the miR-19a-3p binding site. The green asterisk indicates the Zika bases that can interact with miR-19a-3p binding site and are in a highly structure conserved region. Upper Middle: Arc plots showing the RNA-RNA interactions along the ZIKV genome in this region. Lower Middle; Schematic showing the locations along ZIKV genomes that are structurally conserved (light grey), highly structured (dark grey), sequence conserved (teal), and are potentially functional (blue). Bottom: RNAcofold models between 9530-9570/9820-9890 with the potential miR19a-3p binding site. **b**, Bar charts showing the levels of miR-19a-3p and control RNU48 at 0, 2, 16, and 24 hours post-ZIKV infection using qPCR analysis. **c**, Bar chart showing the levels of PTEN 2 hours post ZIKV infection by qPCR analysis. **d**, Boxplot showing distribution in gene expression changes of miR-19a-3p targets and non-targets 2 hours post-ZIKV infection in Huh7 cells.

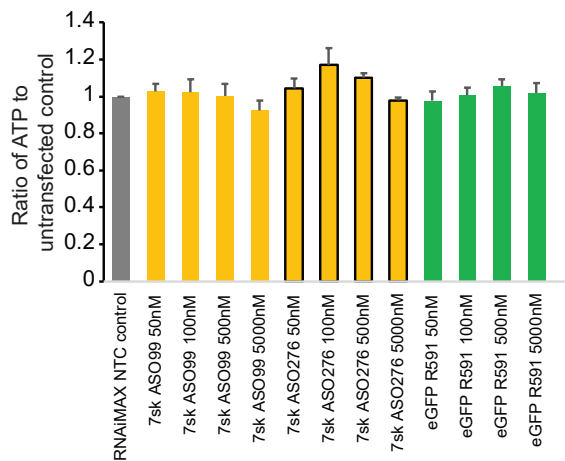
Fig S4

a

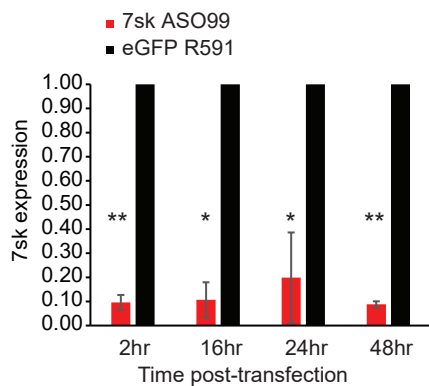
Shared significant host-virus interactions



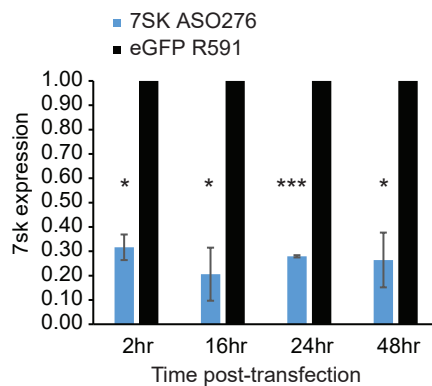
b



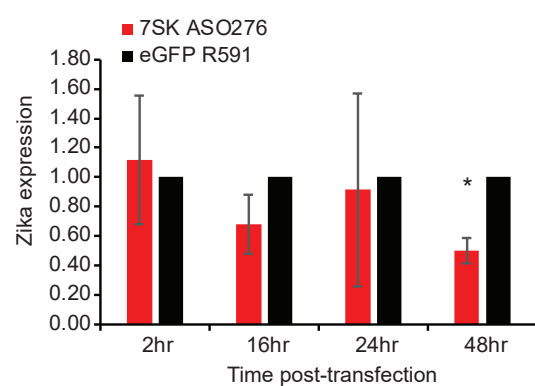
c



d



e



f

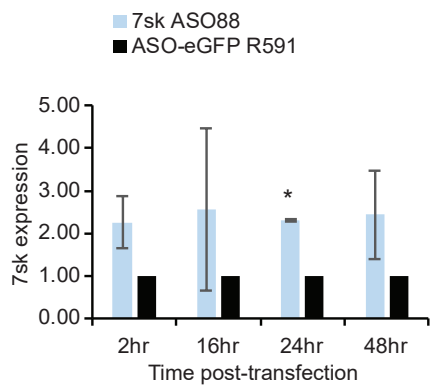


Figure S4. ZIKV:non-coding RNA interaction statistics. **a**, Venn diagram showing the overlap in significant interactions between the different viruses. 32 host RNAs bind to all 5 viruses. **b**, Bar charts showing the average ratio of ATP in cells transfected with different concentrations of ASOs versus ATP in cells that are untransfected. **c,d**, Bar chart showing the levels of 7SK in Huh7 cells 2, 16, 24, 48 hours after transfection of two independent 7SK ASOs, ASO99 (**c**) and ASO276 (**d**) to knock it down. **e**, Bar chart showing the amount of ZIKV present in Huh7 cells 2, 16, 24, 48 hours after 7SK knockdown using ASO276, by qPCR analysis. ZIKV levels are decreased when 7SK levels are decreased. **f**, Bar chart showing the levels of 7SK in Huh7 cells 2, 16, 24, and 48 hours after transfection of 2'O-methylated ASO oligo to 7SK. Transfecting 2'O-methylated ASO against 7SK does not knock down 7SK inside Huh7 cells. **c-f**, *, **, *** indicate p-values ≤ 0.05 , 0.01, and 0.001 respectively, using Student's T-test.

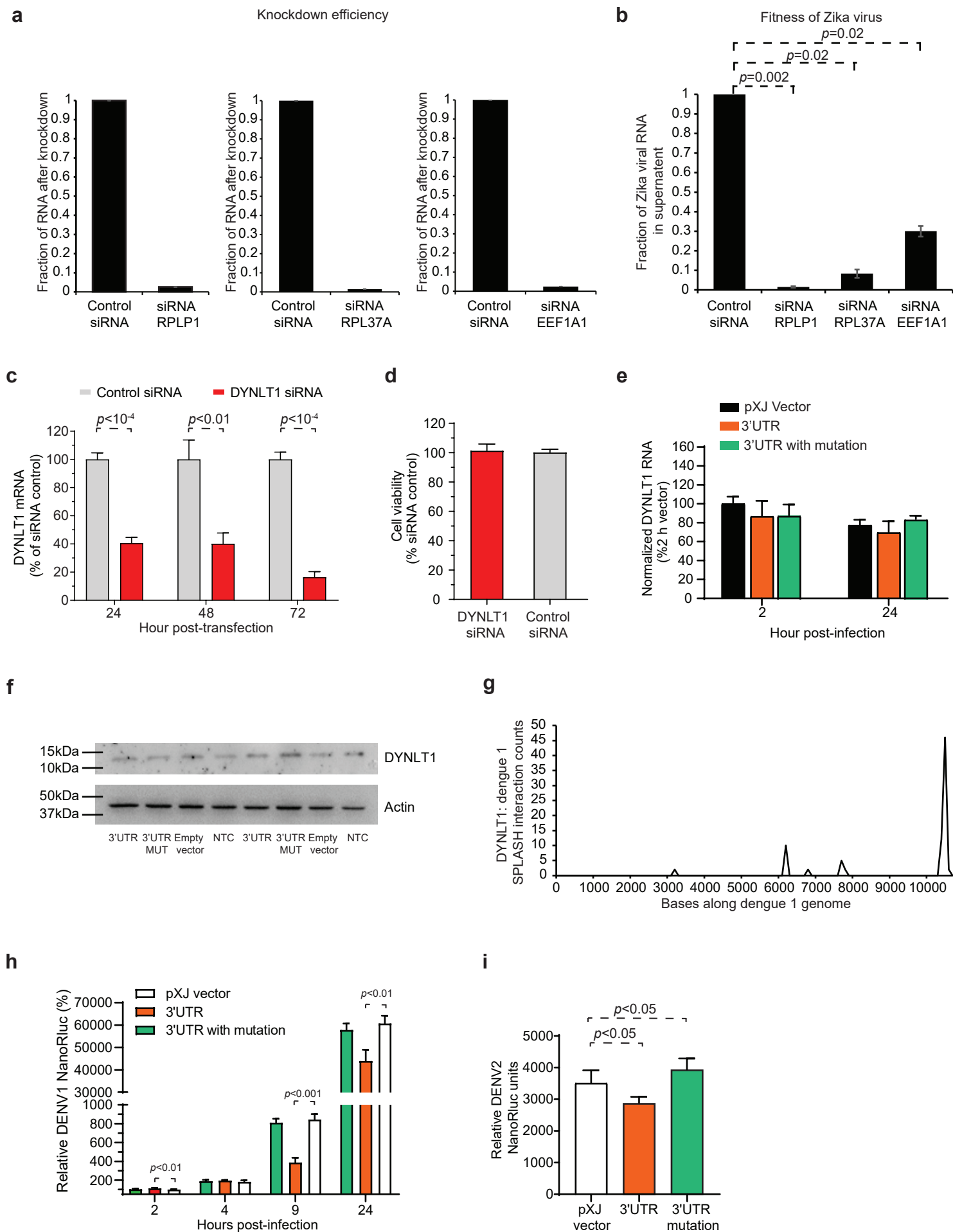
Fig S5

Figure S5. DYNLT1 inhibits DENV and ZIKV replication. **a**, Bar plots showing the knockdown efficiencies of siRNAs against RPLP1, RPL37A, and EEF1A1. All 3 transcripts are knocked down to >90% of their original RNA amount. RPLP1 is a positive control known to affect ZIKV virus replication. RPL37A and EEF1A1 RNAs are identified as interactors of ZIKV RNA. **b**, Bar plots showing the amount of ZIKV virus RNA detected in the supernatant 24 hours post-ZIKV infection, after knockdown of the respective genes. Knockdown of RPL37A and EEF1A1 significantly reduced the amount of virus production from the cells after 24 hours. **c**, Knockdown of DYNLT1 expression after siRNA transfection. Huh7 cells were transfected with 20 nM of DYNLT1 siRNA or a control siRNA. At 24, 48, and 72 h post-transfection, the intracellular DYNLT1 mRNAs were quantified by RT-qPCR. The relative mRNA levels were obtained by normalizing the DYNLT1 mRNAs of each group to those of the siRNA control group. Means and SDs from four independent experiments are presented. **d**, Knockdown of DYNLT1 siRNA does not affect cell viability. Huh7 cells were transfected with 20 nM of DYNLT1 siRNA or a control siRNA. At 48 h post-transfection, cell viability was measured using the CellTiter-Glo® Luminescent cell viability assay. Data were normalized to the control groups. Means and SDs from three independent experiments are presented. **e**, Overexpression of DYNLT1 3'UTR marginally affects endogenous DYNLT1 mRNA. Huh7 cells were transfected with 200 ng of DYNLT 3'UTR, DYNLT1 3'UTR with mutation, or pXJ vector. At 24 h post-transfection, cells were infected with recombinant ZIKV strain PRVABC59 containing a nanoluciferase gene at an MOI of 0.5. At 2 h and 24 h post-infection, the intracellular DYNLT1 mRNAs were quantified by RT-qPCR. The relative mRNA levels were obtained by normalizing the DYNLT1 mRNAs of each group to those of the control group at 2 h post-infection. Means and SDs from four independent experiments are presented. **f**, Western blot showing the protein levels of DYNLT1 in Huh7 cells after overexpression of DYNLT1 3'UTR (lanes 1 and 5), DYNLT1 mutant 3'UTR (lanes 2 and 6), and empty vector (lanes 3 and 7). **g**, Line plot showing the locations along DENV-1 that binds to DYNLT1. The Y-axis indicates the number of interaction counts between DENV-1 and DYNLT1 for that location. **h**, DYNLT1 3'UTR inhibits DENV-1 replication. Huh7 cells were transfected with 400 ng of DYNLT 3'UTR, DYNLT1 3'UTR with mutation, or pXJ vector. At 24 h post-transfection, cells were infected with recombinant DENV-1 strain West Pac containing a nanoluciferase gene at an MOI of 1.0. At given time points, cells were harvested. The relative luciferase signals were obtained by normalizing the luciferase readouts of each group to those of control at 2 h post-infection. Means and SDs from four independent experiments are presented. **i**, DYNLT1 3'UTR suppresses DENV-2 replication. Huh7 cells were transfected with 200 ng of DYNLT 3'UTR, DYNLT1 3'UTR with mutation, or pXJ vector. At 24 h post-transfection, cells were infected with recombinant DENV-2 D2Y98P containing a nanoluciferase gene at an MOI of

1.0. At given time points, cells were harvested. The luciferase signals were measured. Means and SDs from four independent experiments are presented.